Synthesis of water-soluble porphyrin with tyrosine fragments and study of its interaction with S-protein of SARS-CoV-2*

S. A. Syrbu,[a] A. S. Semeikin,[b] N. Sh. Lebedeva,[a] Yu. A. Gubarev,[a]★ E. S. Yurina,[a] S. S. Guseinov,[a] and O. I. Koifman[a,b]

[a]*G. A. Krestov Institute of Solution Chemistry, Russian Academy of Sciences, 1 ul. Akademicheskaya, 153045 Ivanovo, Russian Federation. E-mail: gua@isc-ras.ru*
[b]*Ivanovo State University of Chemistry and Technology, 7 Sheremetevskii prosp., 153000 Ivanovo, Russian Federation*

The multistage purposeful synthesis of 5,15-bis(4′-L-*N*-tyrosinylamidophenyl)-10,20-bis(*N*-methylpyridin-3′-yl)porphine diiodide was carried out, and the optimum synthesis conditions were determined. 5,15-Bis(4′-nitrophenyl)-10,20-bis(pyridin-3′-yl)porphine served as the starting porphyrin. The structure, individual character, and purity of the target compound were proved by electron spectroscopy, ^{1}H NMR spectroscopy, mass spectrometry (MALDI TOF), and TLC. Specific features of the interaction of the synthesized porphyrin with S-protein of SARS-CoV-2 were studied using spectral and thermochemical methods, including conditions of photoirradiation. The photoirradiation of the synthesized porphyrin in a complex with the SARS-CoV-2 S-protein can result in the partial oxidation of amino acid residues of the protein and distort its primary and secondary structures. The photoirradiation of the S-protein complex with the porphyrin decreases its thermal resistance to melting by 15 °C compared to the free S-protein and causes porphyrin release.

Key words: synthesis, water-soluble porphyrin, S-protein, SARS-CoV-2, virucidal effect, photoinactivation.

Coronavirus infection induced by SARS-CoV-2 virus caused a huge economic and social damage. According to the state on June 2022, the COVID-19 pandemic took away more than 6 millions human lives. Efficient drugs capable of withstanding the viral infection are being permanently searched.[1] Photodynamic inactivation of pathogens is considered to be one of the most promising methods. The virucidal effect is based on a photosensitizer that forms a complex with a target (pathogen molecule). Under photoirradiation the photosensitizer generates active oxygen species (AOS) that launch the chain of oxidation reactions leading to virus annihilation. In the case of SARS-CoV-2, S-protein is the most evident target. Being a structural protein that forms spinous sprouts on the virion surface, S-protein provides docking of a viral species with angiotensin-converting enzyme (ACE2) of the host cells, as well as membrane joining and internalization of the virus to the cell. S-Protein is a transmembrane protein consisting of two subunits: (1) subunit S1 responsible for binding with ACE2 (in this case, the genes coding the synthesis of subunit S1 are very prone to mutations) and (2) subunit S2 responsible for membrane joining and considered to be one of conservative regions of S-protein.[2] It is widely known that porphyrin compounds that efficiently absorb light energy and generate singlet oxygen can be used as photosensitizers for the photoinactivation of pathogens.[3—6] Another unambiguous advantage of porphyrins is a possibility of purposeful chemical modification of peripheral substitution to impart required complexation properties to the substance, which would enhance selectivity of the drugs. We have previously[7] determined the structure of the porphyrin compound by quantum chemical methods: 5,15-bis(4′-L-tyrosinylamidophenyl)-10,20-bis-(*N*-methylpyridin-3′-yl)porphine dioidide, whose distinctive feature is binding with the subunit S2 of S-protein of coronavirus. The purpose of this work is

* Based on the materials of the V Russian Conference on Medicinal Chemistry with international participation "MedChem-Russia 2021" (May 16—19, 2022, Volgograd, Russia).

Published in Russian in *Izvestiya Akademii Nauk. Seriya Khimicheskaya,* No. 11, pp. 2495—2504, November, 2022.
1066-5285/22/7111-2495

to develop the synthetic procedure for this porphyrin, to study its interaction with S-protein of SARS-CoV-2 coronavirus, and to evaluate the influence of photoirradiation on the properties of S-protein inside the complex with the synthesized porphyrin.

Results and Discussion

Synthesis of water-soluble 5,15-bis(4′-L-tyrosinylamidophenyl)-10,20-bis(*N*-methylpyridin-3′-yl)porphine diiodide (TyrP, **1**). The starting porphyrin for the synthesis of target compound **1** is 5,15-bis(4-nitrophenyl)-10,20-bis(pyridin-3′-yl)porphine (**2**), which can be prepared by two methods: first, by "mixed-aldehyde" synthesis,[8,9] condensation of pyrrole with a mixture of 4-nitrobenzaldehyde and pyridine-3-carboxaldehyde in propionic acid followed by the separation of a mixture of porphyrins using chromatography, and second, by the condensation of *meso*-(4-nitrophenyl)dipyrrolylmethane, which was synthesized by a previously described procedure,[10] with pyridine-3-carboxaldehyde in propionic acid. The further reduction of compound **2** with tin dichloride in hydrochloric acid similarly to a described method[11] affords 5,15-bis(4-aminophenyl)-10,20-bis(pyridin-3-yl)porphine (**3**) (Scheme 1).

A drawback of the first method is the formation of a poorly separable mixture of six porphyrins in the statistic ratio ($\mathbf{A_4}$, 6.25%; $\mathbf{A_3B}$, 25%; *cis*-$\mathbf{A_2B_2}$, 25%; *trans*-$\mathbf{A_2B_2}$, 12.5%; $\mathbf{AB_3}$, 25%; $\mathbf{B_4}$, 6.25%),[12] and the required porphyrin **2** is formed in lower amounts than the 5,10-isomer slightly discernible from the 5,15-isomer by mobility on a chromatographic column.

The second method is more convenient since should result in only one product: required isomer **2**. However, this reaction in an acidic medium is accompanied by acidolysis processes with the formation of a mixture of porphyrin products with different arrangements of *meso*-substituting groups.[9] We tested the both methods and, as a result, confirmed the drawn conclusions.

Therefore, the condensation of pyridyl-3-carboxaldehyde with *meso*-4-nitrophenyl)dipyrrolylmethane was carried out under the conditions that allow one to avoid acidolysis processes: in pyridine or quinoline at high temperature (Rothemund method[9]) in the presence of zinc acetate as a template agent.

The zinc porphyrin complex was found to simultaneously form an outer-sphere zinc complex with the pyridyl residue, which is insoluble in organic solvents. Hence, the reduction to aminoporphyrin **3** was further carried out without isolation (9% yield based on the starting *meso*-(4-nitrophenyl)dipyrrolylmethane) (see Scheme 1).

Then, the condensation of *meso*-pyridin-3-yldipyrrolylmethane with 4-nitrobenzaldehyde in propionic acid with an additive of propionic anhydride gave porphyrin **2** in the absence of acidolysis products (Scheme 2), which was further reduced by tin dichloride dihydrate in hydrochloric acid to amino derivative **3** similarly to that presented in Scheme 1.

The activation of L-di-BOC-tyrosine (L-*N*,*O*-di-BOC-tyr) with *N*,*N*′-dicyclohexylcarbodiimide (DCC) (Scheme 3) was used for the synthesis of 5,15-bis-

Scheme 1

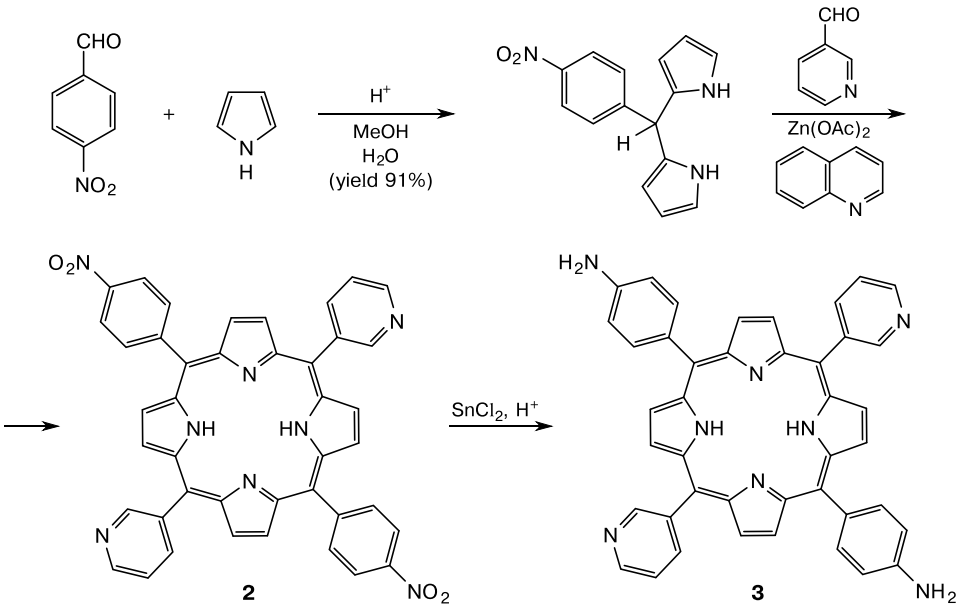

Scheme 2

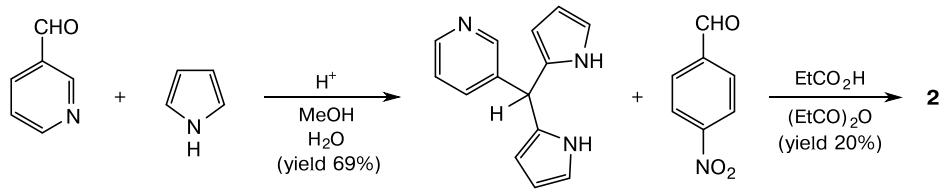

Scheme 3

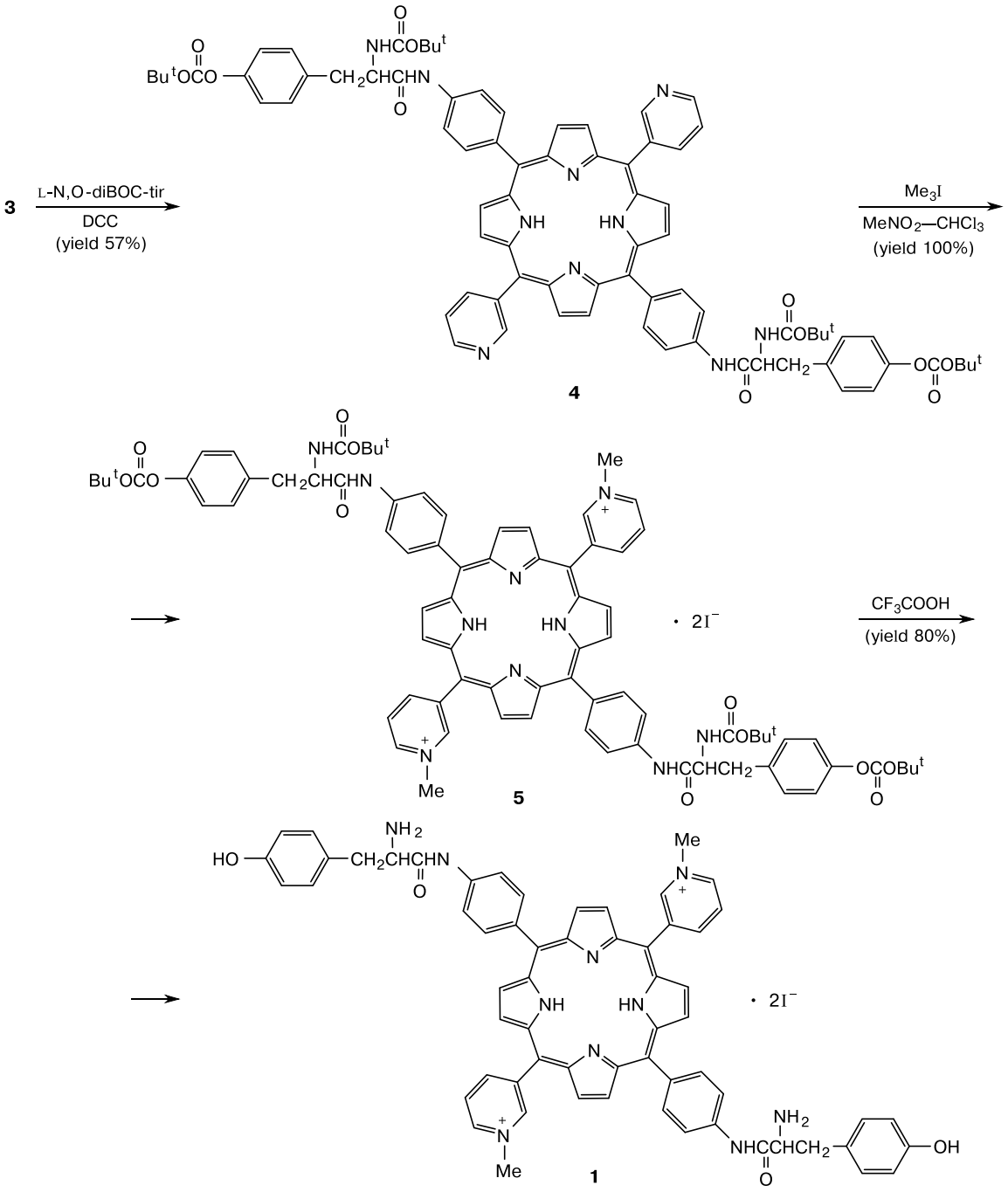

[4′-(L-*N*,*O*-di-*tert*-butyloxytyrosinyl)amidophenyl]-10,20-bis(pyridin-3′-yl)porphine (**4**). To impart solubility in water to compound **4**, that latter was methylated at the pyridyl residues with methyl iodide in a nitromethane—chloroform mixture to 5,15-бис[4′-bis-(*N*,*O*-di-BOC-L-tyrosinyl)amidophenyl]-10,20-bis(*N*-methylpyridin-3′-yl)porphine (**5**) diiodide, and then the BOC protection was eliminated by trifluoroacetic acid to give **1** (see Scheme 3). All synthesized compounds were characterized, and the results are given in Experimental).

Study of the interaction of compound 1 with the SARS-CoV-2 S-protein. The S-protein was synthesized at the N. I. Lobachevsky Nizhny Novgorod State University in *E. coli* cells. After isolation and purification, the S-protein was dissolved in a phosphate-buffered saline (PBS) with pH 7.4. This buffer medium was chosen because the osmolarity and concentration of ions in PBS correspond to the concentrations in the human body; *i.e.*, this buffer solution is isotonic. The electronic absorption spectrum (EAS) and fluorescence spectrum of synthesized compound **1** in PBS indicate that porphyrin **1** in a concentration of $3.5 \cdot 10^{-6}$ mol L^{-1} in this medium exists in the associated state (EAS of porphyrin **3**: broad Soret band, $\lambda_{max} = 453$ nm, $A = 0.08$; nearly no fluorescence). According to the EAS, porphyrin **1** in the same concentration in an osmolar aqueous solution of sodium chloride exists predominantly in the monomeric form (EAS of porphyrin: narrow Soret band, $\lambda_{max} = 417$ nm, $A = 0.48$; fluorescence typical of porphyrin, $\lambda_1 = 652$ nm, $\lambda_2 = 703$ nm). Titration of porphyrin **1** dissolved in water with NaCl (0.15 mol L^{-1}) with a phosphate buffer results in the self-association of porphyrin ($3.5 \cdot 10^{-6}$ mol L^{-1}), which appears as a decrease in the absorption intensity and bathochromic shift of the Soret band from 417 to 432 nm, and the fluorescence of porphyrin is quenched. Taking into account the obtained results and impossibility of avoiding the presence of PBS in the system, the interaction of synthesized porphyrin **1** with S-protein was studied by the titration of porphyrin **1** in an aqueous solution of NaCl (0.15 mol L^{-1}) with S-protein in PBS. The EAS of porphyrin **1** upon titration with S-protein are shown in Fig. 1.

As can be seen from Fig. 1, the titration with S-protein increases light scattering in the studied system and, in addition, induces the aggregation of porphyrin **1** due to the introduction of PBS to the solution. Since the following processes are complicated and mutually dependent:

$$\text{S-Protein} + \mathbf{1}_m \rightleftharpoons \text{S-Protein} \cdot \mathbf{1}_m, \qquad (1)$$

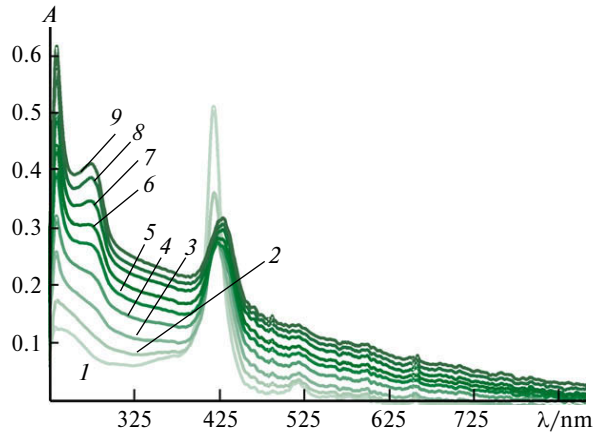

Fig. 1. Electronic absorption spectra of porphyrin **1** in an aqueous solution of NaCl upon titration with S-protein in PBS: *1*, solution of porphyrin **1** in PBS and *2*—*9*, consecutive addition of S-protein.

$$n\mathbf{1}_m \rightleftharpoons \mathbf{1}_{ass}, \qquad (2)$$

where indices "m" and "ass" correspond to the monomer and associate, respectively, it is impossible to obtain quantitative parameters for reaction (1). However, the fact of complex formation can be confirmed by an analysis of the fluorescence quenching rate of porphyrin **1** during its titration with a pure buffer and S-protein in the buffer (Fig. 2). The detected fluorescence spectra were corrected in order to take into account the re-absorption effect. The dependences of the fluorescence quenching rate of porphyrin **1** on the amount of added PBS (curve *1*) or S-protein in PBS (curve *2*) are shown in Fig. 2. It is seen that the introduction of S-protein to porphyrin solutions substantially retards fluorescence quenching; *i.e.*, the presence of the protein shifts equilibrium (2) to the left. The obtained results

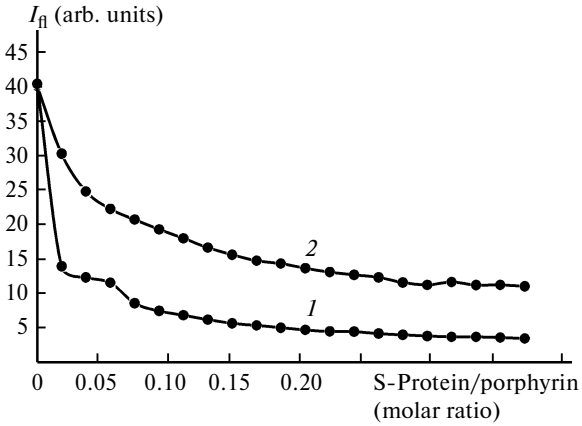

Fig. 2. Fluorescence quenching for porphyrin **1** ($3.5 \cdot 10^{-6}$ mol L^{-1}) upon titration with PBS (*1*) and S-protein ($6.5 \cdot 10^{-8}$—$1.3 \cdot 10^{-6}$ mol L^{-1}) in PBS (*2*).

allow one to conclude about binding of porphyrin **1** by S-protein.

The next stage of the work was the IR spectral study. The IR spectrum of the S-protein complex with porphyrin **1** is not additive to the spectra of the starting reagents. For instance, new bands, which are absent from the IR spectra of the starting reagents, appear at 3493.15 and 846.5 cm^{-1}. Note that the IR spectrum of the protein-containing samples is poorly resolved, and the absorption is broad-band. Upon complex formation, some absorption bands (ν/cm^{-1}) of the protein undergo shifts to the high-frequency range (1534.15 → 1538.92, 2118.38 → 2121.51, 2923.50 → 2926.16, 2955.55 → 2963.56, 3461.49 → 3493.15), whereas another part of the bands shifts to the short-frequency range (478.06 → 473.61, 626.69 → 621.11, 1241.26 → 1231.71, 1776.10 → 1774.51, 2847.36 → 2845.77, 3239.81 → 3236.64, 3392.30 → 3361.23) (Table 1). The listed changes in the IR spectra confirm the complex formation between S-protein and porphyrin **1**. An analysis of the amide ranges in the IR spectra of individual S-protein and inside the complex with porphyrin **1** showed that the binding of porphyrin **1** results, on the whole, in minor changes in the secondary structure of the protein, which is due to both a high molecular weight of the protein (151 kDa) and the local character of the effect of porphyrin **1**. According to the molecular docking results,[7] porphyrin **1** is bound in subunit S2 of the protein, and the secondary structure of subunit S2 is predominantly presented by α-helices. However, these minor changes are distinctly observed in amide range III, and the vibrational band at 1241 cm^{-1} shifts to 1231 cm^{-1}, which corresponds to an increase in the fraction of disordered fragments in the protein.[13–15]

Study of the photochemical properties of porphyrin 1 and its complex with the S-protein of SARS-CoV-2. The quantum yield of singlet oxygen was estimated by

Table 1. IR spectra* (ν/cm^{-1}) of S-protein, porphyrin **1**, complex S-protein · **1**, and irradiated complex S-protein · **1**-*hν*

S-Protein	Porphyrin **1**	Complex S-protein · **1**	Complex S-protein · **1**-*hν*
3927.98 w		3932.57 w	—
3562.82 br.int		3578.66 br.int	3556.9 br.int
—		3493.15 br.int	—
3461.49 br.int	3451.99 v.int	3361.23 br.int	3380.42 br.int
	3416.04 v.int		
3239.81 n.int		3236.64 n.int	3236.64 n.int
	3103.64 w		
	33049.81 vw		
2955.60 w		2963.56 w	2964.30 w
2923.50 w	2923.77 m	2926.16 w	2919.97 w
2847.36 vw	2853.47 w	2845.77 vw	2858.63 vw
2118.33 sh		2121.51 sh	2108.98 sh
2031.73 v.br		2032.01 v.br	2031.78 v.br
1776.10 w		1774.51 w	1770.43 w
1639.20 n.int	1678.46 v.int	1640.31 n.int	1634.26 n.int
1616.68 n.int		1616.38 n.int	1616.53 n.int
1534.15 br.m		1538.92 br.m	1544.67 w
1459.33 w	1488.84 m	1456.92 w	1463.25 w
1400.65 m		1400.45 m	1400.99 m
	1317.42 m		
1241.26 sh	1201.17 n.int	1231.71 sh	1238.51 sh
1141.26 br.int	136.13 n.int	1140.51 br.int	1142.31 br.int
	915.40 w		
—	831.67 m	861.56 m	—
	801.05 m		
	718.69 m		
626.69 br.int	620.94 br.w	639.89 br.int	621.47 br.int
478.96 m		478.38 m	478.38 m

* In KBr, in a range of 4000—400 cm^{-1}.

** The following designations were used: vw is very weak, w is weak, m is medium, int is intense, v.int is very intense, n is narrow, br is broad, and sh is shoulder.

studying the photochemical properties of porphyrin **1**. The yield was 0.77, which lies in the range of quantum yields of photosensitizers used for photodynamic therapy (PDT). Visual blurring was observed after the photoirradiation at λ = 425 nm of solutions of the S-protein complexes with porphyrin **1**, and light scattering increases in the EAS of the complexes. This fact indicates a change in the protein conformation, exposure of hydrophobic residues on the globule surface, and protein aggregation. Probably, the photoirradiation of the complex resulted in the partial oxidation of the amino acid residues situated in the immediate vicinity of porphyrin **1** and, as a consequence, in the violation of the hydrogen bond between the amino acid residues stabilizing the protein conformation.

The IR spectrum of the irradiated S-protein complex with porphyrin **1** differs substantially from the initial IR spectra of the complex and S-protein (see Table 1). Note that the bands appeared upon complex formation disappeared after photoirradiation. Perhaps, the photooxidation of the protein inducing the partial oxidation of amino acid residues and a change in its conformation also led to the destruction of the complex.

To examine the effects observed, it seemed necessary to study the temperature dependence of the specific heat capacity (c_p) of the studied solutions (of the S-protein complex with porphyrin **1** before and after photoirradiation, S-protein, porphyrin **1**, PBS) by heat flow differential scanning calorimetry.

The obtained temperature dependences of the c_p values of the studied solutions are shown in Fig. 3. Below 78 °C, these values change in the order S-protein < **1** < irradiated complex S-protein • **1**-*h*ν < < complex S-protein • **1**.

The following correlation equation was derived for the quantitative estimation of the fraction of structural changes in the solution associated with the irradiation process compared to the starting complex:

$$c_p(\text{S-protein} \cdot \mathbf{1}\text{-}h\nu) = $$
$$= (0.746\pm0.017)c_p(\text{S-protein} \cdot \mathbf{1}) +$$
$$+ (0.257\pm0.012)c_p(\text{S-protein}) + (0.013\pm0.034) \quad \text{(I)}$$
$$(R = 0.9959,\ \text{SD} = 0.0077\ \text{J g}^{-1}\ \text{K}^{-1},\ N = 82).$$

The coefficients at c_p(S-protein • **1**) and c_p(S-protein) in Eq. (I) indicate that the structure of the complex after irradiation differs from the initial structure. According to this model, the fraction of the complex in the initial form equal to 0.746 of the content of the initial complex is retained in the composition of the irradiated complex. The fraction of the structurally changed S-protein inside the complex after irradiation is 0.257. However, it should be mentioned that derived Eq. (I) makes it possible to establish a relationship between the heat capacities of the indicated solutions of the protein, and their main component is the buffer. Correlation equation (II) was derived in which the influence of the buffer was taken into account as the difference of specific heat capacities (Δc_p) of the protein and complexes before and after irradiation minus the heat capacity of the buffer

$$\Delta c_p(\text{S-protein} \cdot \mathbf{1}\text{-}h\nu) = $$
$$= (0.730\pm0.015)\Delta c_p(\text{S-protein} \cdot \mathbf{1}) +$$
$$+ (0.231\pm0.025)\Delta c_p(\text{S-protein}) + (0.022\pm0.004) \quad \text{(II)}$$
$$(R = 0.9686,\ \text{SD} = 0.0076\ \text{J g}^{-1}\ \text{K}^{-1},\ N = 82),$$

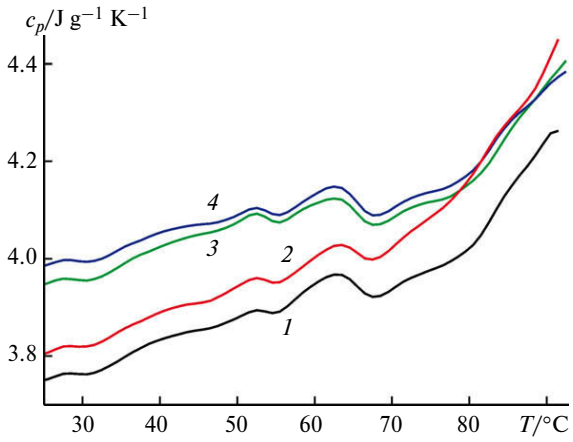

Fig. 3. Temperature dependences of the specific heat capacity (c_p) of solutions of S-protein (*1*), porphyrin **1** (*2*), complex S-protein • **1**-*h*ν (*3*), and complex S-protein • **1** (*4*).

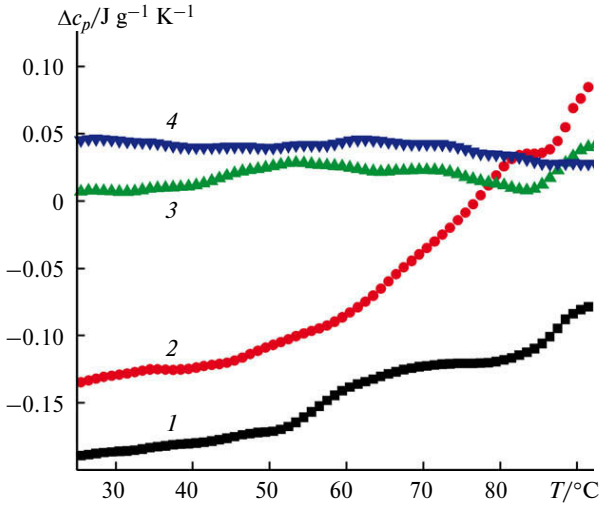

Fig. 4. Temperature dependences of the differences in specific heat capacities (Δc_p^{sp}) of solutions of S-protein (*1*), porphyrin **1** (*2*), complex S-protein • **1** (*3*), and complex S-protein • **1**-*h*ν (*4*) and buffer.

where $\Delta c_p(i) = c_p(i) - c_p(\text{PBS})$ is the difference between the specific heat capacities of solutions of the protein or complex and buffer, respectively.

As can be seen from correlation equations (I) and (II), the coefficients at the corresponding parameters within the inaccuracy coincide, indicating that the chosen model is valid.

The temperature dependence of $\Delta c_p(i)$ (Fig. 4) shows the changes in the heat capacities related to the conformational transitions of S-protein and the S-protein complex with porphyrin **1** before and after irradiation and to the aggregation of porphyrin **1**.

The differences in heat capacities $\Delta c_p(i)$ with allowance for the sign vary in the following sequence: S-protein < **1** < irradiated complex S-protein · **1**-*hν* < < complex S-protein · **1**. As can be seen from Fig. 4, the Δc_p values of S-protein, complex S-protein · **1**, and irradiated complex S-protein · **1**-*hν* nearly linearly change with temperature to 52, 41, and 35 °C, respectively. A vibrational mobility of larger regions of macromolecule-segments appears with the further temperature increases and, as a consequence, with an increase in the intensity of vibrational motions of the atoms and groups composing macromolecules. The appearance of segmental mobility allows conformational transitions to occur for S-protein and its complexes with porphyrin **1**, which induces a sharp change in the heat capacity with changing temperature. The nonlinear changes in Δc_p (see Fig. 4) to 82 °C for the pure protein and irradiated complex and also to 85 °C for the starting complex are characteristic of the melting of the protein. The heat capacity of a solution of porphyrin **1** increases monotonically and nonlinearly with increasing temperature to 82 °C, and then the heat capacity remains nearly constant to 86 °C and then increases linearly to the final temperature; *i.e.*, heat capacity jump is observed. This can be related, on the one hand, to structural changes in the solution favoring an increase in the heat capacity, and on the other hand, to the formation of more stable structures, which results in a decrease in the heat capacity, namely, to the aggregation of porphyrin **1** in the solution. A similar but less pronounced jump is detected on the curve of changing Δc_p for the irradiated S-protein complex with porphyrin **1**. The contribution from the *exo*-process when comparing the Δc_p values for the irradiated S-protein · **1**-*hν* complex with the values for S-protein and complex S-protein · **1** is especially pronounced. It is reasonable to assume that the revealed *exo*-effect is associated with the aggregation of porphyrin **1**. This confirms the conclusions of the IR spectral study (see Table 1) that porphyrin **1** is released along with the partial oxidation of the protein upon the photoirradiation of the complex.

Thus, the synthesis of water-soluble 5,15-bis(4′-L-tyrosinylamidophenyl)-10,20-bis(*N*-methylpyridin-3′-yl)porphine diiodide (**1**) was presented for the first time in this work. The structure of synthesized porphyrin **1** was proved by electron spectroscopy, ^{1}H NMR spectroscopy, and mass spectrometry. The interaction processes of porphyrin **1** with the S-protein of SARS-CoV-2 were studied by spectral and thermochemical methods. The formation of the S-protein complex with porphyrin **1** was found to result in slight changes in the secondary structure of the S-protein and an increase in the fraction of disordered fragments, which, in turn, induces a decrease in the melting point of the S-protein by 11 °C. The photoirradiation of the S-protein complex with porphyrin **1** was shown to induce the partial oxidation of amino acid residues of the protein and to decrease in its thermal resistance to melting by 15 and 6 °C compared to those of the S-protein and starting complex of S-protein with porphyrin **1**, respectively. The photoirradiation of the S-protein complex with porphyrin **1** leads to the release of porphyrin **1**, which can provide the prolonged action of the photosensitizer; *i.e.*, porphyrin **1** released upon photoirradiation can bind to the next non-oxidized biomolecule.

Experimental

Electronic absorption spectra and fluorescence spectra were recorded on a SPEK SSP-715 scanning spectrometer and on an AvaSpec-2048 fiber-optic spectrophotometer (Avantes BV) at 25 °C in quartz cells (1 cm). When studying florescence, monochromatic light diodes with maxima at 295 and 525 nm served as exciting light sources. ^{1}H NMR spectra were studied on a Bruker 500 spectrophotometer (500.0 MHz) at the Center for Collective Use of Scientific Equipment "Upper Volga Regional Center of Physicochemical Investigation" of the G. A. Krestov Institute of Solution Chemistry of the Russian Academy of Sciences. ^{13}C NMR spectra were not obtained because of low solubility of the compounds. Mass spectra were detected on a Shimadzu Axima Confidence time-of-flight mass spectrometer (MALDI-TOF) at the Center for Collective Use of the Ivanovo State University of Chemistry and TechnologFor solutions with the absorbances higher than 0.1 at the irradiation wavelength, fluorescence was corrected according to the equation

$$F_{\text{corr}(\lambda)} = F_{\text{obs}(\lambda)} \cdot 10^{[A_{\text{ex}(\lambda\text{ex})} + A_{\text{em}(\lambda)}]/2},$$

where $F_{\text{corr}(\lambda)}$ and $F_{\text{obs}(\lambda)}$ are the corrected and observed fluorescence at the corresponding wavelength, respectively; $A_{\text{ex}(\lambda\text{ex})}$ and $A_{\text{em}(\lambda)}$ are the absorbance of the solution at the excitation wavelength and at the wavelength under study.[16]

Thermochemical studies were carried out on a DSC 204 F1 heat flow differential scanning calorimeter (Netzsch Gerätebau GmbH, Germany). Samples (solutions) 20—25 mg in weight were placed in pressed aluminum crucibles. An empty aluminum crucible served as the reference sample. Calorimetric experiment was conducted in a dynamic atmosphere of dry argon (argon content 99.998%) with a flow rate of 40 mL min^{-1} and a heating rate of 1 °C min^{-1} in the temperature range from 12 to 93 °C. All measurements were carried out relative to the base line obtained for two empty crucibles. The temperature and sensitivity of the calorimeter were calibrated by measuring temperatures and enthalpies of phase transitions for 11 standard substances: Hg, C_6H_{12}, $C_{12}H_{10}$, KNO_3, $RbNO_3$, In, Bi, Sn, Zn, $KClO_4$, and CsCl. The accuracy of temperature measurement was 0.1 °C, and the weighing accuracy was ±0.01 mg (Sartorius M2P Balance). The DSC curves were used for the calculation of the specific heat capacity of protein solutions: base line, standard, and sample. Sapphire served as the standard. All the three measurements were carried out sequentially for 1 day. Multiparametric correlation dependences (I) and (II) were calculated according to the DSC data in the Origin 7.5 program package from the temperature dependences of the heat capacities (number of points $N = 82$).

The quantum yield of singlet oxygen was determined for the photolysis of 1,3-diphenylisobenzofuran[17] in air-saturated DMF by the equation

$$\Phi_\Delta = \Phi_\Delta{}^{Std} R I_{abs}{}^{Std} / (R^{Std} I_{abs}),$$

where $\Phi_\Delta{}^{Std}$ is the quantum yield of singlet oxygen of 5,10,15,20-tetraphenylporphyrin, which is equal[18] to 0.64 in DMF; R^{Std} and R are the photolysis rates of 1,3-diphenylisobenzofuran in the presence of the standard and studied substance, respectively; $I_{abs}{}^{Std}$ and I_{abs} are the amounts of light absorbed by the standard and studied substance, respectively; and the amount of light was determined radiometrically on an AvaSpec-2048 spectrophotometer (Avantes BV). The study was carried out as follows: the solvent (1.45 mL) was placed in a cell with a stirrer, a light diode was switched on, and the amount of light passed through the diode in the range of diode emission (450—600 nm) was measured. Then, a solution of porphyrin **1** (25 μL) was added in such a way that the absorbance at the wavelength 525 nm would be about 0.3, and the amount of light passed through the solution in a range of 450—600 nm was determined. The amount of light absorbed by the solution was determined as the difference in the amounts of light passed through the pure solvent and a solution of porphyrin **1**. Then, 1,3-diphenylisobenzofuran (25 μL) was added to the solution until the concentration achieved 0.09 mmol L^{-1}, and the absorption spectra were recorded upon the irradiation with the diode at an interval of 10 s. The initial stage of the process when no more than 10% 1,3-diphenylisobenzofuran decomposed was used to calculate the photolysis rate.

IR spectra were recorded on an Avatar 360 FT-IR spectrometer (Thermo Nicolet, USA) in a range of 4000—500 cm^{-1} in KBr. To prepare samples, solutions of S-protein with porphyrin **1** in PBS were mixed in a molar ratio of 1 : 1 and solutions of the starting reagents and complex were evaporated at room temperature to a constant weight. The prepared samples were triturated with KBr and pressed in pellets.

***meso*-(4-Nitrophenyl)dipyrrolylmethane.** Pyrrole (2.8 mL, 40.4 mmol) and then 4-nitrobenzaldehyde (2.0 g, 13.2 mmol) were added with stirring to a solution of concentrated hydrochloric acid (1.5 mL) in 100 mL of water (~0.18 *M* solution). The reaction mixture was stirred for 2 h, and the precipitate was filtered off, washed with water, and dried. The yield was 3.2 g (90.7%). The product was recrystallized from methanol. ^{1}H NMR ($CDCl_3$), δ: 8.16 (d, 2 H, H(3), H(5), Ph, $J = 8.7$ Hz); 8.00 (br.s, 2 H, NH); 7.39 (d, 2 H, H(2), H(6), Ph, $J = 8.7$ Hz); 6.74—6.78 (m, 2 H, Pyr); 6.16—6.20 (m, 2 H, Pyr); 5.87—5.90 (m, 2 H, Pyr); 5.60 (s, 1 H, *ms*-H). Mass spectrum: found *m/z* 267.0112 $[M + H]^+$; calculated for $C_{15}H_{13}N_3O_2$ 267.2835.

***meso*-(Pyrid-3-yl)dipyrrolylmethane.** Pyrrole (5.0 mL, 72.22 mmol) and pyridine-3-carbaldehyde (2.3 mL, 24.37 mmol) were gradually added with stirring to a solution of concentrated hydrochloric acid (5.0 mL) in water (200 mL). The reaction mixture was stirred for 2 h and slowly neutralized with a concentrated solution of ammonia (5.5 mL, 73.47 mmol) in water (25 mL). The precipitate was filtered off, washed with water, milled in a mortar under a water layer, filtered again, and dried at room temperature in air. The yield was 4.5 g (68.8%). ^{1}H NMR ($CDCl_3$), δ: 8.49 (dd, 1 H, H(6), Py, $J_1 = 4.7$ Hz, $J_2 = 1.3$ Hz); 8.45 (d, 1 H, H(2), Py, $^3J = 1.9$ Hz); 8.27 (br.s, 2 H, NH); 7.54 (d, 1 H, H(5), Py, $^4J = 8.0$ Hz, $^3J = 1.9$ Hz); 7.27 (dd, 1 H, H(4), Py, $^4J_1 = 8.0$ Hz, $J_2 = 4.7$ Hz); 6.76 (dd, 2 H, Pyr, $^5J = 4.1$ Hz, $^6J = 2.6$ Hz); 6.19 (dd, 2 H, Pyr, $^7J = 5.9$ Hz, $^8J = 2.9$ Hz); 5.88—5.91 (m, 2 H, Pyr); 5.49 (s, 1 H, *ms*-H). Mass spectrum: found *m/z* 223.4284 $[M + H]^+$; calculated for $C_{14}H_{13}N_3$ 223.2715.

5,15-Bis(4′-nitrophenyl)-10,20-bis(pyridin-3′-yl)porphine (2). A solution of *meso*-(pyridin-3-yl)dipyrrolylmethane (4.5 g, 20.15 mmol) and 4-nitrobenzaldehyde (3.2 g, 21.17 mmol) in a mixture of propionic acid (100 mL) and acetic anhydride (10 mL, 0.106 mol) was refluxed for 1.5 h. Then the solvent was distilled off *in vacuo*, and the residue was diluted with water and neutralized with an ammonia solution. The precipitate was filtered off, washed with water, and dried in air at 70 °C. The residue was extracted in a Soxhlet apparatus with chloroform with an additive of triethylamine (2 mL) until the formation of a colorless leaking out solution. The extract was chromatographed on alumina (activity grade II) eluting with chloroform with 1% ethanol. The eluate was evaporated, and porphyrin was precipitated with petroleum ether, filtered off, washed with petroleum ether, and dried in air at 70 °C. The yield was 1.45 g (20.4%); R_f (Alufol): 0.88 (benzene—methanol (20 : 1)). EAS, λ_{max}/nm (log ε): 647 (3.83); 590 (3.94); 551 (4.06); 516 (4.33); 420 (5.51) (chloroform). ^{1}H NMR ($CDCl_3$), δ: 9.48 (s, 2H, H(2), Py); 9.11 (dd, 2 H, H(4), Py, $J_1 = 5.0$ Hz; $J_2 = 1.6$ Hz); 8.89 (d, 4 H, H(2), H(8), H(12), H(18), $J = 4.4$ Hz); 8.85 (d, 4 H, H(3), H(7), H(13), H(17), $J = 4.4$ Hz); 8.69 (d, 4 H, H(2), H(6), Ar, $^3J = 7.8$ Hz); 8.55 (d, 2 H, H(6), Py, $^4J = 7.6$ Hz, $^1J = 1.6$ Hz); 8.43 (d, 4 H, H(3), H(5), Ar, $^3J = 7.8$ Hz); 7.81

(dd, 2 H, H(5), Py, ^4J = 7.6 Hz, J = 5.0 Hz); –2.79 (br.s, 2 H, NH). Mass spectrum: found m/z 708.0131 $[M + H]^+$; calculated for $C_{42}H_{26}N_8O_4$ 706.7104.

5,15-Bis(4-aminophenyl)-10,20-bis(pyridin-3-yl)porphine (3). Method *A*. A solution of *meso*-(4-nitrophenyl)dipyrrolylmethane (1 g, 3.96 mmol), 3-pyridinecarbaldehyde (1 mL, 10.60 mmol), and anhydrous zinc acetate (0.5 g, 2.73 mmol) in quinoline (10 mL, 84.61 mmol) was refluxed for 9 h. The reaction mixture was cooled down and poured to water, and quinoline was distilled off with water vapor. The residue was filtered off, washed with water, and dried in air at 70 °C. The residue was refluxed for 0.5 h with 2 g (8.86 mmol) of tin chloride dihydrate and 6.0 mL (38.72 mmol) of concentrated hydrochloric acid in methanol (50 mL). The solution was cooled down, diluted with water, filtered, and neutralized with a solution of potassium hydroxide (10 g, 0.178 mol) in water (50 mL). The precipitate was filtered off, washed with water, and dried in air at 70 °C. The residue was dissolved in boiling chloroform, filtered, and chromatographed on alumina (activity grade II) eluting with chloroform. The porphyrin eluate was evaporated and precipitated with petroleum ether. The precipitate was filtered off, washed with petroleum ether, and dried in air at 70 °C. The yield was 120 mg (9.4%).

Method *B*. A mixture of compound **2** (1.5 g, 2.12 mmol) and tin chloride dihydrate (6.0 g, 26.59 mmol), concentrated hydrochloric acid (10 mL), and water (15 mL) in methanol (100 mL) was refluxed for 1 h. The solution was cooled down and filtered, and the precipitate was washed with water with hydrochloric acid until a colorless leaking out solution formed, diluted with water by 50%, and neutralized with stirring with a solution of potassium hydroxide (25.0 g, 0.446 mol) in water (50 mL). The precipitate was filtered off, washed with water, and dried in air at 70 °C. The residue was washed in a Soxhlet apparatus until a colorless leaking out solution formed. The solution was cooled down and chromatographed on alumina (activity grade II) eluting with chloroform. The porphyrin eluate was evaporated and precipitated with petroleum ether. The precipitate was filtered off, washed with petroleum ether, and dried in air at 70 °C. The yield was 0.73 g (53.2%); R_f (Silufol): 0.87 (benzene—methanol (2 : 1)). EAS, λ_{max}/nm (log ε): 653 (3.80); 596 (5.4); 560 (4.0); 521 (4.15); 426 (5.44) (chloroform). Mass spectrum: found m/z 647.6760 $[M + H]^+$; calculated for $C_{42}H_{30}N_8$ 646.7623. ^{1}H NMR (DMSO-d_6), δ: 9.38 (s, 2 H, 2-Py); 9.06 (d, 2 H, 6-Py, J = 4.9 Hz); 9.00 (d, 4 H, β-H, J = 3.3 Hz); 8.79 (d, 4 H, β-H, J = 3.3 Hz); 8.66 (d, 2 H, 4-Py, J = 8.7 Hz); 7.91 (t, 2 H, 5-Py, J = 6.4 Hz); 7.87 (d, 4 H, H(2), H(6), Ar, J = 7.8 Hz); 7.02 (d, 4 H, H(2), H(6), Ar, J = 7.8 Hz); 6.61 (br.s, 4 H, NH_2); –2.80 (br.s, 2 H, NH).

5,15-Bis[4′-(L-*N*,*O*-di-*tert*-butyloxytyrosinyl)amidophenyl]-10,20-bis(pyridin-3′-yl)porphine (4). DCC (120 mg, 0.58 mmol) was added with stirring ice-cooling to a solution of L-*N*,*O*-di-BOC-tyrosine (200 mg, 0.52 mmol) and 4-*N*,*N*-dimethylaminopyridine (60 mg, 0.50 mmol) in dried chloroform (10 mL). The reaction mixture was stirred on cooling with ice for 2 h, 5,15-bis(4′-aminophenyl)-10,20-bis(pyridin-3′-yl)porphine (50 mg, 77.3 μmol) was added, the mixture was stored with stirring (TLC control) for 2 days, and DCC (200 mg) was additionally added. The mixture was stirred for 1 day more, filtered, and chromatographed on alumina (activity grade II) eluting with chloroform with 1% ethanol. The eluate was evaporated, and the product was precipitated with petroleum ether, filtered off, and dried. The yield was 70 mg (56.6%); R_f (Silufol): 0.58 (benzene—methanol (10 : 1)). EAS, λ_{max}/nm (log ε): 652 (3.68); 594 (3.71); 553 (3.89); 619 (4.12); 422 (5.49) (chloroform). Mass spectrum: found m/z 1375.5884 $[M + H]^+$; calculated for $C_{80}H_{80}N_{10}O_{12}$ 1373.5736. ^{1}H NMR ($CDCl_3$), δ: 9.46 (s, 2 H); 9.07 (d, 2 H, J = 4.2 Hz); 8.94 (d, 4 H, J = 4.0 Hz); 8.81 (d, 4 H, J = 4.0 Hz); 8.25 (m, 4 H); 8.17 (d, 4 H, J = 7.7 Hz); 7.43 (d, 4 H, H(2), H(6), Ar, J = 8.1 Hz); 7.25 (d, 4 H, H(3), H(5), Ar, J = 8.1 Hz); 7.16 (d, 4 H, H(3), H(5), Ar′, J = 8.4 Hz); 7.12 (d, 4 H, H(2), H(6), Ar′, J = 8.4 Hz); 6.52 (d, 4 H, J = 5.5 Hz); 5.29 (br.s, 2 H); 5.02 (d, 2 H, J = 8.3 Hz); 4.66 (br.s, 2 H); 4.56 (q, 2 H, J = 7.2 Hz); 4.18 (q, 4 H, J = 7.2 Hz); 3.33 (m, 4 H); 3.10 (dd, 2 H, J = 6.2 Hz); 1.58, 1.57 (both s, 36 H, Bu^t); 1.55 (s, 20 H, Bu^t); 1.45 (s, 16 H, Bu^t); –2.82 (br.s, 2 H, NH).

5,15-Bis[4′-bis(*N*,*O*-di-BOC-L-tyrosinyl)amidophenyl]-10,20-bis(*N*-methylpyridin-3′-yl)porphine diiodide (5). A solution of compound **4** (90 mg, 0.066 mmol) in a mixture of methyl iodide (2 mL, 32.11 mmol), dried nitromethane (5 mL), and dried chloroform (10 mL) was refluxed for 4 h. Then the mixture was cooled down, poured onto a Petri dich, and dried in air. The yield was 110 mg (100%). EAS, λ_{max}/nm (log ε): 659 (3.75); 595 (3.90); 563 (3.98); 525 (4.20); 431 (5.27) (chloroform). Mass spectrum: found M_{exp} 1405.2541; calculated for $C_{82}H_{86}N_{10}O_{12}$ 1403.6437.

5,15-Bis(4′-bis-L-tyrosinylamidophenyl)-10,20-bis(*N*-methylpyridin-3′-yl)porphine diiodide (1). A solution of compound **5** (110 mg, 0.066 mmol) in trifluoroacetic acid (4 mL) was stirred for 4 h, kept for ~14 h, then poured onto a watch crystal, and dried in air. The yield was 80 mg (80%); R_f (Silufol): ~0.05 (methanol). EAS, λ_{max}/nm (log ε): 646 (3.69); 589 (3.84); 550 (3.90); 514 (4.22); 421 (5.41) (chloroform). Mass spectrum: found M_{exp} 1004.9206; calculated for $[C_{62}H_{54}N_{10}O_4]^{2+}$ 1003.1825. ^{1}H NMR (methanol-d_4), δ: 9.87 (s, 2 H, H(2), Py); 9.35 (d, 4 H, H(6), Py, J = 6.1 Hz); 9.34 (d, 2 H, H(4), Py, J = 7.9 Hz); 9.04—8.86 (m, 8 H, β-H); 8.50 (t, 2 H, H(5), Py, J = 6.6 Hz); 8.17 (d, 4 H, H(2), H(6), Ar, J = 8.4 Hz); 7.98 (d, 4 H, H(3), H(5), Ar, J = 8.4 Hz); 7.17 (d, 4 H, H(2), H(6), Ar-Tyr, J = 8.3 Hz); 8.78 (d, 4 H, H(3), H(5), Ar-Tyr, J = 8.3 Hz); 4.78 (s, $C\underline{H}_3OH$); 4.71 (s, 6 H, NCH_3); 4.26 (t, 2 H, CH-Tyr, J = 6.7 Hz); 3.24—3.30 (m, 2 H, NH); 3.22 (br.s, $CH_3O\underline{H}$).

This work was financially supported by the Russian Foundation for Basic Research (Project No. 20-04-60067). Some research works was carried out using resources of the Upper Volga Regional Center of Physicochemical Research at the G. A. Krestov Institute of Solution Chemistry of the Russian Academy of Sciences and the Center for Collective Use at the Ivanovo State University of Chemistry and Technology.

No human or animal subjects were used in this research.

The authors declare no competing interests.

References

1. A. V. Nemukhin, B. L. Grigorenko, S. V. Lushchekina, S. D. Varfolomeev, *Russ. Chem. Bull.*, 2021, **70**, 2084; DOI: 10.1007/s11172-021-3319-8.
2. M. Takeda, *Microbiol. Immunol.*, 2022, **66**, No. 1, 15; DOI: 10.1111/1348-0421.12945.
3. N. Lebedeva, Y. Gubarev, M. Koifman, O. Koifman, *Molecules*, 2020, **25**, 4368; DOI: 10.3390/molecules25194368.
4. N. S. Lebedeva, O. I. Koifman, *Russ. J. Bioorg. Chem.*, 2022, **48**, 1; DOI: 10.1134/S1068162022010071.
5. O. I. Nikolaeva, T. A. Ageeva, O. I. Koifman, *Russ. Chem. Bull.*, 2021, **70**, 1822; DOI: 10.1007/s11172-021-3288-y.
6. S. S. Shatokhin, V. A. Tuskaev, S. C. Gagieva, É. T. Oganesyan, *Russ. Chem. Bull.*, 2021, **70**, 1011; DOI: 10.1007/s11172-021-3183-6.
7. O. I. Koifman, T. A. Ageeva, I. P. Beletskaya, A. D. Averin, A. A. Yakushev, L. G. Tomilova, T. V. Dubinina, A. Yu. Tsivadze, Yu. G. Gorbunova, A. G. Martynov, D. V. Konarev, S. S. Khasanov, R. N. Lyubovskaya, T. N. Lomova, V. V. Korolev, E. I. Zenkevich, T. Blaudeck, Ch. von Borczyskowski, D. R. T. Zahn, A. F. Mironov, N. A. Bragina, A. V. Ezhov, K. A. Zhdanova, P. A. Stuzhin, G. L. Pakhomov, N. V. Rusakova, N. N. Semenishyn, S. S. Smola, V. I. Parfenyuk, A. S. Vashurin, S. V. Makarov, I. A. Dereven´kov, N. Zh. Mamardashvili, T. S. Kurtikyan, G. G. Martirosyan, V. A. Burmistrov, V. V. Aleksandriiskii, I. V. Novikov, D. A. Pritmov, M. A. Grin, N. V. Suvorov, A. A. Tsigankov, A. Yu. Fedorov, N. S. Kuzmina, A. V. Nyuchev, V. F. Otvagin, A. V. Kustov, D. V. Belykh, D. B. Berezin, A. B. Solovieva, P. S. Timashev, E. R. Milaeva, Yu. A. Gracheva, M. A. Dodokhova, A. V. Safronenko, D. B. Shpakovsky, S. A. Syrbu, Yu. A. Gubarev, A. N. Kiselev, M. O. Koifman, N. Sh. Lebedeva, E. S. Yurina, *Macroheterocycles*, 2020, **13**, 4; DOI: 10.6060/mhc200814k.
8. A. Semeikin, in *Uspekhi khimii porfirinov* [*Advances in the Chemistry of Porphyrin*], Ed. O. A. Golubchikov, NII Khimii SPbGU, St. Petersburg, 1997, p. 52 (in Russian).
9. A. S. Semeykin, S. A. Syrbu, O. I. Koifman, in *Chemical Processes with Participation of Biological and Related Compounds*, Eds T. N. Lomova, G. E. Zaikov, Brill, The Netherlands, 2008, p. 45.
10. E. Dolušić, H. T. Ngo, W. Maes, W. Dehaen, *Arkivoc*, 2007, **10**, 307; DOI: 10.3998/ark.5550190.0008.a20.
11. M. A. Salnikova, T. V. Lubimova, A. V. Glazunov, S. A. Syrbu, A. S. Semeikin, *Macroheterocycles*, 2014, **7**, 249; DOI: 10.6060/mhc140510s.
12. P. Laszlo, J. Luchetti, *Chem. Lett.*, 1993, **22**, 449; DOI: 10.1246/cl.1993.449.
13. K. C. Bauer, S. Suhm, A. K. Wöll, J. Hubbuch, *Int. J. Pharm.*, 2017, **516**, 82; DOI: 10.1016/j.ijpharm.2016.11.009.
14. D. M. Byler, H. Susi, *Biopolymers: Original Research on Biomolecules*, 1986, **25**, 469; DOI: 10.1002/bip.360250307.
15. A. Dong, B. Kendrick, L. Kreilgård, J. Matsuura, M. C. Manning, J. F. Carpenter, *Arch. Biochem. Biophys.*, 1997, **347**, 213; DOI: 10.1006/abbi.1997.0349.
16. N. S. Lebedeva, Y. A. Gubarev, E. S. Yurina, S. A. Syrbu, *J. Mol. Liq.*, 2018, **265**, 664; DOI: 10.1016/j.molliq.2018.06.030.
17. A. Ogunsipe, T. Nyokong, *J. Mol. Struct.*, 2004, **689**, 89; DOI: 10.1016/j.molstruc.2003.10.024.
18. A. B. Ormond, H. S. Freeman, *Dyes Pigm.*, 2013, **96**, 440; DOI: 10.1016/j.dyepig.2012.09.011.

Received June 10, 2022;
in revised form August 15, 2022;
accepted September 19, 2022